#### **PAPER**

# Simulation of many-body dynamics using Rydberg excitons

To cite this article: Jacob Taylor et al 2022 Quantum Sci. Technol. 7 035016

View the article online for updates and enhancements.

# You may also like

- An insect-scale robot reveals the effects of different body dynamics regimes during open-loop running in feature-laden terrain Perrin E Schiebel, Jennifer Shum, Henry Cerbone et al.
- Bipedal Walking Based on Body Dynamics Using Phase Oscillator: Robustness against gentle Ascent
- T. Kinugasa, T. Tada, Y. Yokoyama et al.
- Universal many-body response of heavy impurities coupled to a Fermi sea: a review of recent progress
  Richard Schmidt, Michael Knap, Dmitri A

Ivanov et al.



# IOP ebooks™

Bringing together innovative digital publishing with leading authors from the global scientific community.

Start exploring the collection-download the first chapter of every title for free.

# Quantum Science and Technology



#### **PAPER**

# Simulation of many-body dynamics using Rydberg excitons

7 July 2021 REVISED

22 March 2022

ACCEPTED FOR PUBLICATION 18 May 2022

PUBLISHED
6 June 2022

Jacob Taylor<sup>1,2,6</sup>, Sumit Goswami<sup>3,6</sup>, Valentin Walther<sup>4</sup>, Michael Spanner<sup>1,5</sup>, Christoph Simon<sup>3</sup> and Khabat Heshami<sup>1,5</sup>

- National Research Council of Canada, 100 Sussex Drive, Ottawa, Ontario K1A 0R6, Canada
- <sup>2</sup> University of Waterloo, 200 University Ave W, Waterloo, Ontario N2L 3G1, Canada
- <sup>3</sup> Institute for Quantum Science and Technology and Department of Physics and Astronomy, University of Calgary, Calgary T2N 1N4, Alberta, Canada
- <sup>4</sup> ITAMP, Harvard-Smithsonian Center for Astrophysics, Cambridge, MA 02138, United States of America
- Department of Physics, University of Ottawa, 25 Templeton Street, Ottawa, Ontario, K1N 6N5 Canada
- \*Author to whom any correspondence should be addressed.
- 6 These authors contributed equally to this work.

E-mail: khabat.heshami@nrc-cnrc.gc.ca

Keywords: quantum many-body dynamics, Rydberg excitons, quantum simulation, light-matter interaction, Rydberg dynamics

#### **Abstract**

The recent observation of high-lying Rydberg states of excitons in semiconductors with relatively high binding energy motivates exploring their applications in quantum nonlinear optics and quantum information processing. Here, we study Rydberg excitation dynamics of a mesoscopic array of excitons to demonstrate its application in simulation of quantum many-body dynamics. We show that the  $\mathbb{Z}_2$ -ordered phase can be reached using physical parameters available for cuprous oxide (Cu<sub>2</sub>O) by optimizing driving laser parameters such as duration, intensity, and frequency. In an example, we study the application of our proposed system to solving the maximum independent set problem based on the Rydberg blockade effect.

# 1. Introduction

The strong dipole transition between high-lying Rydberg states of atoms is the origin of the long-range interaction between Rydberg atoms [1, 2]. The most notable manifestation of Rydberg–Rydberg interaction is the Rydberg blockade effect where exciting one atom prevents all other atoms in a certain vicinity from being excited to the same Rydberg state [3, 4]. This feature has inspired several applications in quantum nonlinear optics [5] for development of single photon sources [6], photon–photon gates [7], and switches [8]. The application of Rydberg blockade effect has also been explored in generation of entangled states of atoms for atomic clocks [9] and for entanglement distribution in quantum repeaters [10, 11]. Progress in trapping individual atoms combined with the ability to controllably excite atoms to their Rydberg states is enabling applications in quantum simulation of quantum many-body dynamics [12, 13] and in generation of many-body entangled states [14]. Rydberg atoms in an optical lattice and the blockade effect provide the opportunity to unlock their applications in finding quantum simulation solutions for mathematical problems such as the maximum independent set (MIS) problem [15].

Bound states of electron–hole pairs (excitons) in semi-conductors are governed by the Coulomb attraction and therefore demonstrate properties similar to those of hydrogen-like atoms. In semiconductors with a relatively high exciton binding energy Rydberg states of excitons can be observed. In [16], the authors observed Rydberg states of excitons in cuprous oxide (Cu<sub>2</sub>O) and the effect of Rydberg blockade on the absorption spectroscopy outcome. This work sparked new interest in characterizing Rydberg excitons such as their scaling properties [17], interaction coefficients [18, 19], broadband spectroscopy [20], electro-magnetic properties [21] and temperature dependence of the optical lines [22]. With experimental progress toward micro-structures [23] and ideas on strain-induced trapping of Rydberg excitons [24] there is an increased motivation to explore applications of Rydberg excitons. In particular, Rydberg excitons in various semiconductors have the potential for applications in quantum non-linear optics [25, 26], photonic quantum information processing, and in quantum simulation [27].

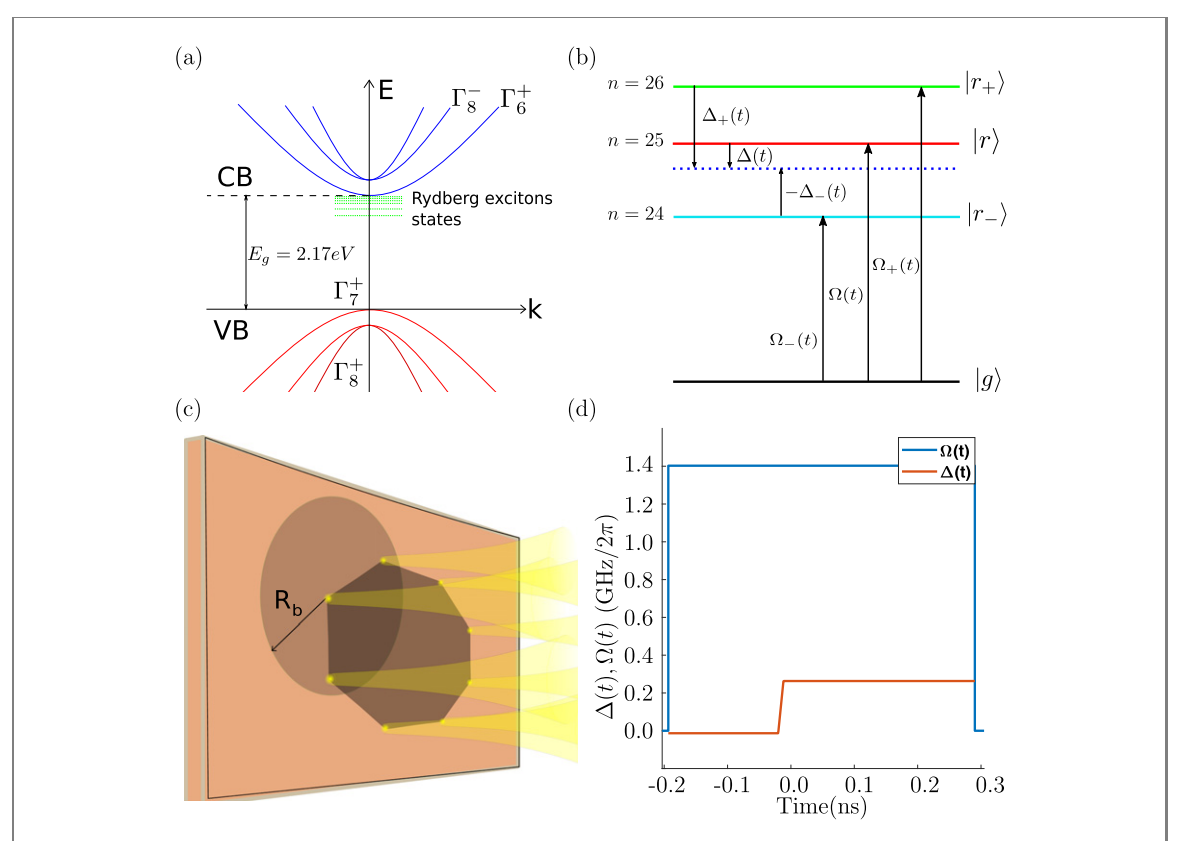


**Figure 1.** (a) Energy band structure of yellow excitons in Cu<sub>2</sub>O (CB = conduction band and VB = valence band), (b) a diagram of the level structure for a single exciton in the case of three Rydberg levels, namely the n=24, n=25 and n=26 states; nS states are accessible through a two-photon excitation mediated by the 2P state (not shown here). The effective Rabi frequency experienced by different states ( $\Omega_k(t)$ ) varies due to their different transition dipole moments. (c) Schematic diagram showing how multiple exciton sites, in a regular polygon configuration, are created by focused laser excitations at selective positions in a Cu<sub>2</sub>O micro-crystal. The blockade radius  $R_b$  of one exciton is shown which encompasses its nearest neighbors. (d) The shape of Rabi frequency and detuning with time to the n=25 level is shown here.

Here, we numerically simulate the many-body dynamics resulting from exciting an array of Rydberg excitons in  $Cu_2O$ . Our approach enables us to find optimal experimental conditions for quantum simulation of many-body dynamics or to reach exotic quantum states. In particular, we demonstrate that driving laser intensity, frequency and focusing can be controlled to reach the  $\mathbb{Z}_2$ -ordered quantum many-body state [12]. In an example, we show the application of our proposed system to finding the solution to the MIS problem based on the Rydberg excitation pattern in a two-dimensional arrangement of Rydberg excitons. Our proposed implementation is inspired by the progress in the Rydberg excitation of individually trapped atoms, offers a path for realization in a solid-state system with potential for integration, and provides a platform to explore many-body quantum dynamics with Rydberg excitons.

Scheme. The schematic of cuprous oxide's (Cu<sub>2</sub>O) band structure with bound Rydberg exciton states below the conduction band is shown in figure 1(a). These states can be addressed both through single-photon [16] and two-photon [28] transitions. We aim to address nS states which can be achieved with a two-photon transition via an off-resonant coupling to the 2P (intermediate) state; see figure 1(b). The lack of directionality in the Rydberg–Rydberg interaction between nS states enables us to consider various geometries and to eliminate complications arising from angle-dependent interaction between nP states. The excitons could be arranged in a polygon configuration (figure 1(c)) or for that matter in any arbitrary configuration. This is discussed in more detail below. In figure 1(b), we show how neighboring Rydberg states are addressed with an effective Rabi frequency (intermediate state 2P). As shown in figure 1(c), each excitation site is driven by a focused laser and all sites are exposed to a global secondary exciting laser. Each site is used to define a qubit;  $|g\rangle$  and  $|r\rangle$  are the states of the qubit where  $|g\rangle$  represents lack of an exciton and  $|r\rangle$  an exciton in the Rydberg level.

As shown in figure 1(b), each exciton is treated as a multi-level system being addressed with an effective Rabi frequency resulting from two driving lasers. This is in particular important for Cu<sub>2</sub>O where Rydberg states have relatively small energy spacing. At each site, the lasers are focused in a tiny spot on a very thin crystal such that a small crystal volume—smaller than the Rydberg blockade volume—is illuminated prohibiting multiple excitations in one site. Figure 1(d) shows an example profile for the effective Rabi frequency and two-photon detuning pertaining to our numerical results that are discussed below.

The paper is organized as follows. After the introduction in section 1, section 2 presents the model for our quantum simulation and discusses the results for a polygon configuration of excitons. We discuss the potential practical application of our scheme to solve MIS problems in section 3. Section 4 depicts the road ahead for the implementation of our model. There a comparison is made with the atomic case with directions for future improvement, and challenges like losses and various other issues associated with implementation are discussed. We conclude in section 5 by summarizing our results.

#### 2. Simulation

We study the many-body Rydberg excitation dynamics under the influence of population dynamics and Rydberg–Rydberg interaction. An exciton in the Rydberg level has a large dipole moment which prohibits an excitation within a certain distance, called blockade radius ( $R_b$ ). In our scheme (see figure 1(c)), the blockade radius  $R_b$  contains the neighboring exciton site but not the next nearest-neighbour site. Hence, the Rydberg blockade effect blocks the two nearest neighbors from being excited together creating the  $\mathbb{Z}_2$ -ordered phase, i.e. states of the form  $|rgrgrgr...\rangle$  or  $|grgrgrg...\rangle$ . Similar to these  $\mathbb{Z}_2$ -ordered states, our general objective states are the states with the maximum number of excitations that can occur without any additional excitations within the blockade radius of a Rydberg exciton. Our numerical treatment of the many-body dynamics aims to find the optimum pulse energy and detuning to reach these objective states with the highest probability of success. To afford numerical simulation of several multi-level systems we do not include the effect of excitation decay. To circumvent this limitation, we operate at a fast excitation regime where the total population dynamics remains faster than the expected lifetime of the Rydberg states; see below for a more detailed discussion.

The excitons are detected by applying a detection laser (de-excitation) pulse to take them to the 2P state and then collecting the photons emitted from the 2P exciton decay. Collection fibers and detectors can be placed behind every site to collect emitted photons. Low exciton detection efficiency through this approach can limit scalability of our proposal when multiple photon emissions and detections are required; see the MIS problem in the application section 3. See section 4.3 for an alternative detection scheme.

In our proposal based on Cu<sub>2</sub>O, excitons in nS states, can only be excited via two-photon excitation in a ladder configuration through the intermediate P states, owing to the selection rules. Off-resonant coupling to the transition that promotes an exciton to the 2P state provides the flexibility to operate at various wavelengths. The two-photon excitation scheme [29, 30] off-resonantly through an intermediate state (e.g. the 2P state) can help circumvent the underlying phonon-assisted absorption [16]. This approach is expected to enable sharp two-photon transitions with optical depth and Rydberg blockade properties comparable to that of cold atomic ensembles [29]. For the single-photon detuning of  $\delta$  with respect to the  $|2P\rangle$ , the effective Rabi frequency representing the coupling to the  $|nS\rangle$  is given by  $\Omega = \Omega_1\Omega_2/\delta$ , where  $\Omega_{1,2} = \langle E_{1,2} \cdot d_{g2P,2PnS} \rangle / 2\hbar$ . Here  $E_{1,2}$  are electric field associated with the two excitation fields and  $d_{ij}$  is the transition dipole moment for  $|g\rangle \to |2P\rangle$  and  $|2P\rangle \to |nS\rangle$  transitions. The ground state here represents a lack of exciton and the mode is determined by that of the  $E_1$ . For large  $\delta$  (i.e.  $\delta \gg \Omega_1, \Omega_2$ ), we can describe the two-photon transition with the effective Rabi frequency,  $\Omega$ . Such two-photon excitation was long used to excite nS Rydberg excitons [28] with optical and infrared lasers. A degenerate two-photon excitation with a laser at 1 eV could simplify the experimental condition. Resonant coupling to the intermediate state is also a possibility based on electromagnetically induced transparency as explored in [26, 29]—using an optical and another THz laser—to show enhanced non-linearity through Rydberg excitons in an optical cavity.

Contrary to the Rydberg atoms, in  $Cu_2O$  excitons, the separation between Rydberg levels is not much greater than the linewidth of these levels. The smaller ratio of line separation and linewidth is a major challenge for effective excitation of  $Cu_2O$  excitons to a single Rydberg level; which can be important for quantum information processing applications. While trying to excite the intended excited state (say, n=25) we may inadvertently excite adjacent levels too (n=24, n=26 etc). This significantly decreases the probability of achieving the objective state(s) in the  $Cu_2O$  exciton system compared to the atomic system, as discussed later. Hence, this effect is needed to be included for an effective simulation of the quantum dynamics. For this purpose, we model each  $Cu_2O$  exciton as a four-level system, one ground and three Rydberg levels system as shown in figure 1(b). We aim to excite the n=25 level. For this high lying Rydberg level (n=25) the energy gaps to the adjacent Rydberg levels are relatively small,  $2\pi \times 2.81$  GHz above and  $2\pi \times 3.18$  GHz below [16] while the linewidth of n=25 level is around  $2\pi \times 0.102$  GHz.

In our model, each exciton is driven by a laser with kth Rydberg state coupled by effective Rabi frequency  $\Omega_k(t)$  and detuning  $\Delta_k(t)$ . The interaction potential between two excitons at ith and jth position is modeled by the principal number dependent van der Waals interaction  $V_{kij} = \frac{C_k}{R_{ij}^6}$ , where  $R_{ij}$  is the distance between the two excitons and  $C_k$  is the interaction coefficient corresponding to the kth Rydberg level.

The Hamiltonian governing such a system is given by

$$\frac{H}{\hbar} = \sum_{k,i} \frac{\Omega_k(t)}{2} (\sigma_i^k) - \sum_{k,i} \Delta_k(t) n_i^k + \sum_{k,i>j} V_{kij} n_i^k n_j^k, \tag{1}$$

where  $|g_i\rangle$  and  $|r_i^k\rangle$  represent the lack of an exciton and an exciton in kth Rydberg level respectively at the ith position (site) in the arrangement.  $\sigma_i^k = |r_i^k\rangle \langle g_i| + |g_i\rangle \langle r_i^k|$ ,  $n_i^k = |r_i^k\rangle \langle r_i^k|$ , and  $V_{kij}$  is the interaction potential between excitons i and j. Interactions between all exciton pairs are considered in our model irrespective of the distance between them. Although larger distance means greatly decreased interaction potential as  $V_{kij} \propto \frac{1}{R_{ij}^6}$ , where  $R_{ij}$  is the distance between excitons i and j. As it can be seen in equation (1), the interaction between different Rydberg states such as 24S–25S is not included in this model. Such cross-interaction terms brings a breadth of possibilities specially in study of wave-packet dynamics in Rydberg excitons where a superposition of multiple Rydberg states of the same exciton is present [19]. Here, we minimize excitation to states other than the targeted 25S state numerically to eliminate the effect of these cross-interaction terms. However, as stated earlier we include the neighboring 24S and 26S states in our simulation all through to show that Rydberg blockade effects are achieved successfully in their presence.

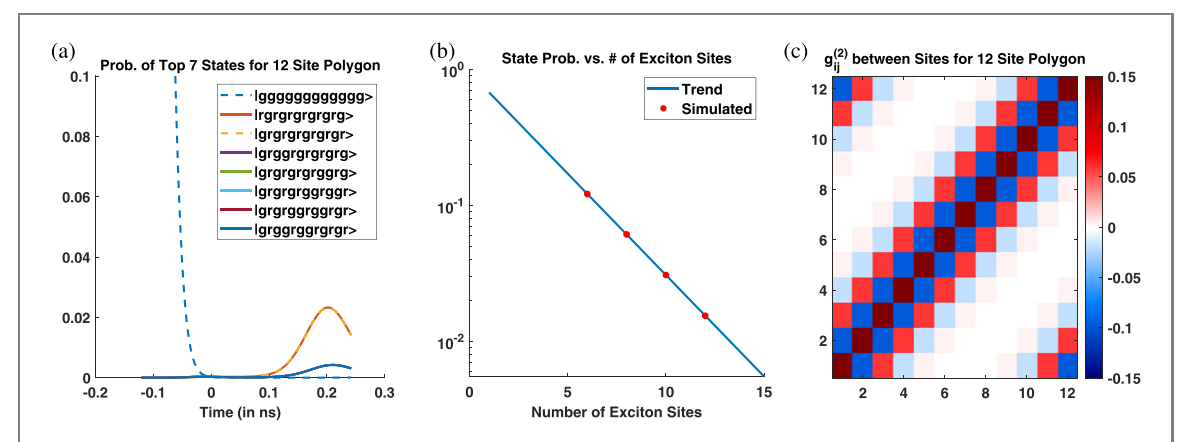
Using a reference Rydberg state, the detuning with respect to the other adjacent states,  $\Delta_{k'-1}$  and  $\Delta_{k'+1}$ , are calculated from the energy gaps [16]. Thus given k' as a reference level,  $R_y$  the Rydberg constant and  $\delta_p$  the quantum defect,  $\Delta_k(t)$  is calculated as  $\Delta_k(t) = \Delta_{k'}(t) + \frac{R_y}{(k'-\delta_p)^2} - \frac{R_y}{(k-\delta_p)^2}$ . Similarly we calculate the Rabi frequency for each Rydberg level using a set of Rabi frequencies and the relative electric dipole moments  $(\mu_k)$ , given a reference k' then  $\Omega_k(t) = \sqrt{\frac{\mu_k}{\mu_{k'}}}\Omega_{k'}(t)$ . In our case the reference k' is the k'=25 state, for all parameters. We propose the same square pulse for all the lasers, so the Rabi frequency is constant in time and space  $(\Omega'_k = \Omega)$  with  $\Omega = 2\pi \times 1.404$  GHz, while  $\Delta(t)$  is time dependent and is iteratively optimized to maximize the probability of reaching a selected objective state(s). In particular  $\Delta(t) = at^3 + bt + c$  is selected where a, b, c are constants optimized for a small system size (such as 5) which is then used for the computation of larger site systems. This  $\Delta(t)$  is also truncated from above/below by  $\Delta_{\max}$ ,  $\Delta_{\min}$  respectively, are selected as to minimize the excitation of neighboring states. The shape of  $\Omega(t)$  and  $\Delta(t)$  used for the simulations are shown in figure 1(d).

We choose the distance between two excitons (i.e. the nearest neighbor distance) as a fraction of the blockade radius. The blockade radius is the distance between the exciton sites such that  $V_{ij} = \Omega$ , or more directly  $R_{\rm b} = \sqrt[6]{\frac{C_6}{\Omega}}$ . The distance was chosen to be about  $0.958 \times R_{\rm b} = 2.72~\mu{\rm m}$  [18]. By having the exciton sites separated by this distance, nearest neighbors have  $V_{k_{ij}} \gg \Omega_k$ , while second nearest neighbor have  $\Omega_k >> V_{k_{ij}}$ . This effect, referred to as Rydberg blockade, blocks nearest neighbors from becoming excited. This was done with the goal of obtaining an ordered objective state(s).

Our objective state(s) refers to the state(s) with the maximum number of excitations that can occur without any nearest neighbors being excited for any arrangement of the exciton sites. Hence, in our simulation where 12 exciton sites are arranged in a regular polygon, the objective states would consist of two states— $|rgrgrgrgrgrg\rangle$  and  $|grgrgrgrgrgr\rangle$ . When the sites in a polygon are excited by lasers a superposition of these states should ideally be the final state of the system with high probability. We numerically simulated this dynamics. The state probabilities are plotted over time in figure 2(a). The objective states for the 12-site polygon are the most probable states. In figure 2(a), we show the population dynamics for generation of the objective states with any of the three neighboring Rydberg states excited. As we aim to minimize Rydberg excitation in neighboring states this is relatively close to dynamics of generating the objective state with a specific Rydberg state denoted as  $|r_1gr_1 \dots gr_1g\rangle$  and  $|gr_1g \dots r_1gr_1\rangle$ .

The maximum probability of the objective state(s)  $(|r_1gr_1...gr_1g\rangle)$  and  $|gr_1g...r_1gr_1\rangle)$  decreases with more exciton sites, as shown in figure 2(b). For a set of 6, 8, 10, and 12 exciton sites probabilities to achieve the objective state are 0.1214, 0.061 27, 0.030 82 and 0.015 45, respectively. Here, it should be noted although the shape of  $\Delta(t)$  with time is optimized to get the highest probability, the same  $\Delta(t)$  profile was used for all the different exciton sites. This is to ensure scalability of our approach so that the optimization results can be applied to higher number of excitons where solving the population dynamics become intractable.

The probabilities in figure 2(b), similar to the system of individually trapped atoms (see figure 4 in reference [12]), shows a clear exponential trend. Extrapolating this trend we calculate that a polygon of 50 exciton sites would be expected to attain the objective state with a probability of around  $P = (3.30 \pm 0.07) \times 10^{-8}$ . This estimate is motivated by the experimental demonstration of the many-body ordered phase in an array of individually trapped atoms [12] and will allow us to gain perspective over our numerical results.



Full quantum state tomography remains very challenging as it requires a high number of complementary measurements. An alternative and very important metric to measure the ordered objective state is by measuring the second order Rydberg–Rydberg correlation function defined as

$$g_{ii}^{(2)} = \langle n_i n_j \rangle - \langle n_i \rangle \langle n_j \rangle, \tag{2}$$

where the average  $(<\cdots>)$  is taken over many repetitions. The blockade effect is apparent within figure 2(c) where a positive value implies correlation while negative value implies anti-correlation. The anti-correlation between the neighboring sites and the correlation between next-nearest neighbors shows a critical signature of the  $\mathbb{Z}_2$ -ordered phase induced by Rydberg blockade between the nearest neighbors. We also see correlation in top-left or bottom-right corner of figure 2(c) because the arrangement here is periodic—e.g. site 1 is also the neighbor of site 12 and hence they are correlated.

Although the objective states we expect ( $|rgrgrgrgrgrg\rangle$  and  $|grgrgrgrgrgr\rangle$ )—described as the  $\mathbb{Z}_2$  order in [12]—has complete correlations, these only occurs with probability  $2 \times 0.015$  while other states with partial or no correlation also occur (figure 2(a)). As the correlation function,  $g^{(2)}$ , is averaged over many runs of the simulation it dies down quickly after a few sites. This is expected and similar results occurred in trapped atom simulation experiments [12]. However, this makes  $g^{(2)}$  an interesting and accessible experimental signature as this correlation can be seen even in the presence of significant loss.

## 2.1. Limited lifetime of excitons and uncertainty in their position

Our approach above is based on two simplifying assumptions. First, we did not include the effect of limited lifetime of the Rydberg states of excitons in favor of gaining the ability to numerically treat a larger number of Rydberg excitons. Second, we consider a point-like positioning for the excitons. This does not include uncertainty in position of each exciton which could potentially degrade efficacy of the Rydberg blockade. In this subsection, we include these effects in our simulations to examine the validity of our assumptions in the earlier results.

In figure 3, we show results of solving the master equation numerically for a system of four excitons. Similar to part (a) in figure 2, we show the top seven most probable states with and without decay. We use the same physical parameters used in the case of 12 exciton polygon. Comparing the results with and without including the limited lifetime (decay) of the states, we can see that the ordered states (the targeted phase) remain to be the states with the most likelihood of occurring. This is re-assuring that our approach based on operating at timescales much faster than the exciton lifetime is effective.

Given the sensitivity of the Rydberg interaction with respect to Rydberg–Rydberg separation, uncertainty in the position of the Rydberg excitons could have implications for the Rydberg blockade effect. Such uncertainty could be caused by the transverse intensity profile of the excitation laser. In figure 4, we consider variations in positioning of Rydberg excitons in a 2D plane. We still use equation (1) (i.e. a point-like representation of the Rydberg exciton) and average over the outcomes for various positions with a Gaussian distribution of width 1  $\mu$ m. As it can be seen in figure 4(b), variation in position of the

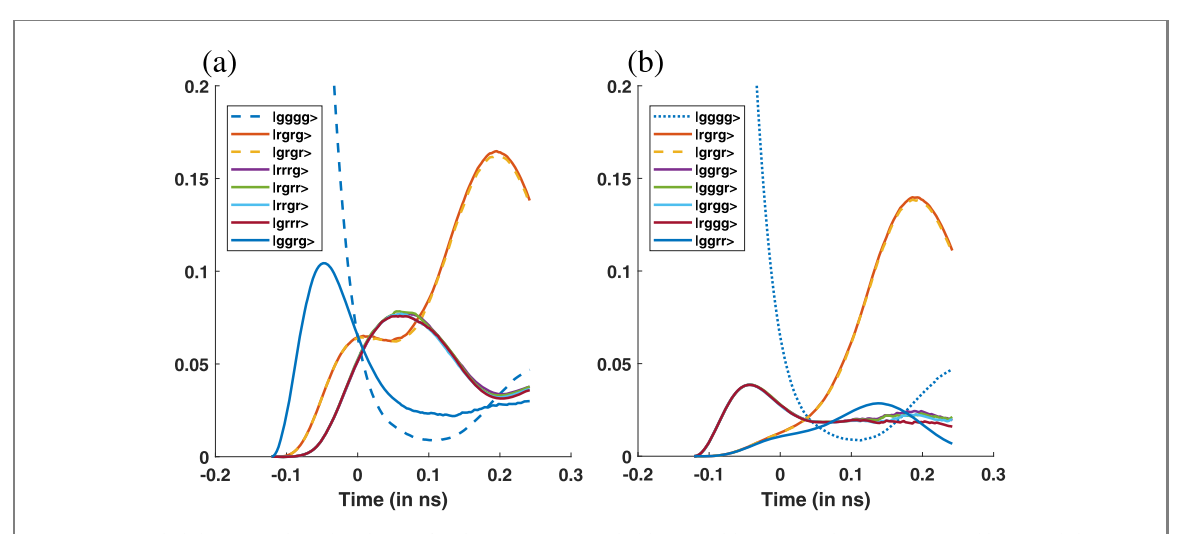


**Figure 3.** Probabilities are plotted with time for the seven most probable ensemble states in the computational basis and the initial state with no excitons,  $|gggg\rangle$  (dashed blue line), for four exciton sites in a polygon configuration. For four sites the most probable states,  $|rgrg\rangle$  and  $|grgr\rangle$  are equally likely. Using an identical pulse sequence to that shown in figure 1(d), the dynamics were simulated (a) without dissipation and (b) with dissipation averaging over 1000 quantum trajectories.

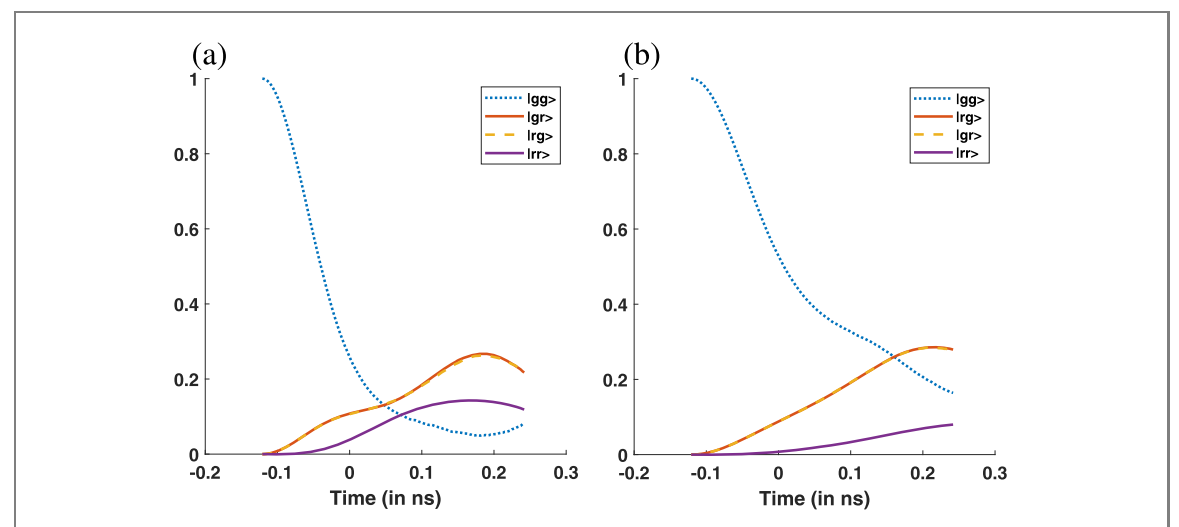


**Figure 4.** Probabilities are plotted with time for two exciton sites for a pulse sequence identical to figure 1(d) where part (a) is for fixed points  $0.958 \times R_b = 2.72~\mu m$  apart or (b) is averaging over a Gaussian position distribution of width 1  $\mu m$  centered on those fixed points, where 100 sample positions were randomly selected.

Rydberg exciton is on average slightly improving the efficiency of the Rydberg blockade. This is a relatively simple check to ensure our assumptions earlier in the results section are reliable. A more elaborate treatment would involve including a spatially varying wavefunction for each exciton. Such a treatment would allow one to explore coherent spatial effects on Rydberg–Rydberg dynamics.

# 3. Application

MIS problem aims to find the largest subset of nodes in a graph where no two nodes are adjacent (linked by an edge). It has been shown that solution to NP-complete problems such as the MIS problem on planar graphs can be mapped onto the ground state of a multi-body Rydberg system with proper arrangement of Rydberg atoms (or in our case excitons); see [31]. This ground state is our objective state with maximum number of Rydberg excitations such that no two excitations occur within the Rydberg blockade radius. If there are two excitations within the blockade radius the total energy goes up and it is no more the ground state. The Rydberg blockade effect combined with a proper positioning of Rydberg excitons will allow us to naturally reach a solution for the MIS problem. Finding the correct position for each Rydberg exciton is an exponentially challenging task for large graphs. Below we treat an example with a graph of ten nodes as shown in figure 5(a).

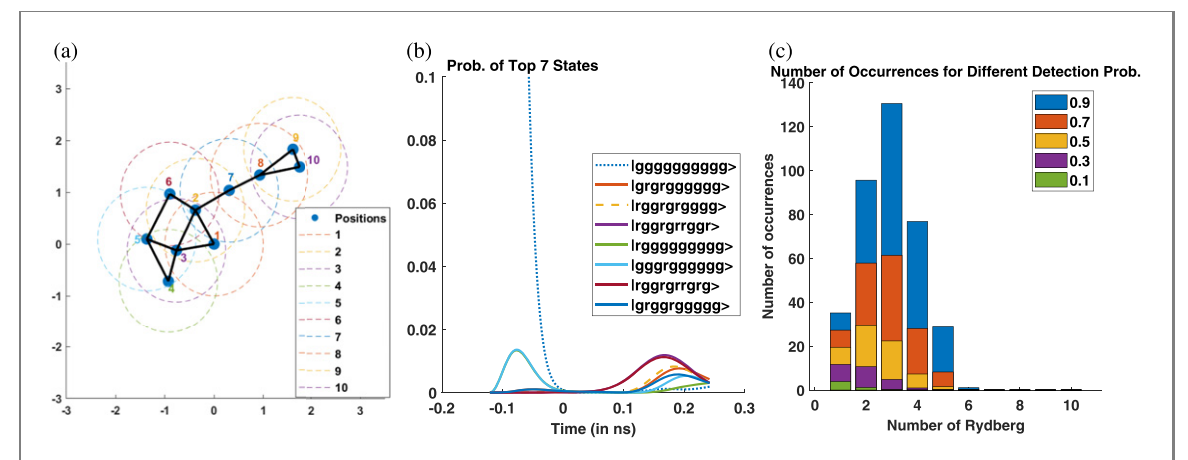


**Figure 5.** (a) A ten site graph with sites arranged arbitrarily in 2D to solve a MIS problem using the excitons. The blockade radius of each exciton is shown by a dotted circle around it and if the separation between two excitons is less than the blockade radius they are connected by an edge creating the graph. (b) Probabilities over time of achieving different states for the ten site graph. The probability of achieving the MIS objective states was found to be 0.011 87 and 0.011 24, with a total probability of 0.023 11. (c) The number of occurrences for different amounts of Rydberg excitons, based off 2000 runs. The histogram is shown for expected number of detections given non-unitary detection probabilities of 0.9, 0.7, 0.5, 0.3 and 0.1.

The polygon scheme described before was a trivial MIS configuration, with the objective state easy to find theoretically. Although we observed that the probability of achieving the objective state is not very high in one repetition of the experiment— $P = 2 \times 0.015$  for 12 sites in a polygon case—that would not eliminate our ability to find a solution as a solution is easy to check in polynomial time. Given a solution one simply needs to check if two of the excitations are within blockade radius—if not it is a 'valid' solution and one looks for the valid solution with maximum number of excitations. All that would be required is enough experimental runs to have a high enough confidence there is no 'valid' larger set of excitations.

We depict such an MIS case in figure 5. Part (a) shows the ten exciton configuration arbitrarily placed in 2D with the solid lines showing the associated planar graph. The evolution of different possible final states of the exciton ensemble are shown in figure 5(b). The objective states (which are called 'ground states' in [31]) with the maximum possible five excitons each, |rggrgrrggr\rangle and |rggrgrrgrg\rangle, have the highest probabilities, 0.011 87 and 0.011 24, with a total probability of 0.023 11. The number of Rydberg excitation in the final state is plotted as an histogram in figure 5(c) over 2000 runs. We see a finite number of occurrences for five excitons but six excitons also occur in small number (at detection efficiency 0.9). Creation of six excitons is an error due to the presence of other nearby Rydberg states (see, figure 1(b)). It can be easily checked that no state associated with six excitation is 'valid', as defined earlier. So, we conclude the five excitation states are our objective (ground) states. Figure 5(c) shows the effect of finite detection efficiencies too, as Rydberg excitation numbers are indicated in different color for different detection efficiencies. Naturally, for lower detection efficiencies we expect to detect smaller number of excitons as more excitons in the final state remain undetected. Low detection efficiency limits us in finding the objective state with maximum number of excitons; however, as it can be seen in figure 5 even for a detection efficiency of 0.7, 2000 runs (attempts) is enough to find the solution to the associated MIS problem. The objective state can be found at even lower detection efficiencies by increasing the number of runs.

## 4. Implementation

# 4.1. Comparison with atoms and improvements

In the following, a comparative analysis is drawn between Rydberg atoms and Rydberg excitons (in Cu<sub>2</sub>O) for their application as a quantum simulator. This will allow us to put our results in perspective and motivate experimental efforts based on Rydberg excitons. Significant progress in trapping individual atoms and well-known Rydberg properties and excitation strategies puts the atomic systems at a significant advantage. However, the relatively slow trapping, excitation, and detection steps (in order of milliseconds) can become a bottleneck in applications that require sampling over many outcomes. On the other hand, for the fast exciton system trapping is not required which will offer simplicity and operation time in the order of nanoseconds.

The closely placed absorption lines of Rydberg excitons (in  $Cu_2O$ ) prohibit effective excitation of Rydberg states resulting in low probability of success in achieving the objective state. The probabilities achieved in our Rydberg exciton simulation are much lower than what is achievable with trapped atoms

[12]. In Cu<sub>2</sub>O excitons, the radiative linewidth of n=25 state is  $2\pi \times 0.102$  GHz as compared to the  $2\pi \times 2.81$  GHz line separation between n=25 and n=26 levels. The linewidth is further broadened due to power broadening effects. The small line-separation limits the range of  $\Omega$  that can be used. To generate the objective state one must prevent excitations into higher/lower Rydberg levels (n=24,26 in our model). It is therefore desirable to have  $\Delta_k > \Omega_k$  for  $k \neq 25$ . In sharp contrast, this condition is very easily satisfied in the atomic system where the atomic linewidth is millions of times smaller than the line separation. Fortunately, this large linewidth and hence the small lifetime of excitons is not without benefits, as it also allows many iterations of the experiment to be performed orders of magnitude faster than individually trapped Rydberg atoms. Operating on orders of nanoseconds instead of  $100~\mu s$ , as in the atoms. This allows one to do 100~000~s of times more repetitions in the same time, increasing the number of successful attempts in generating the objective state. This in turn increases the probability of a successful detection and hence identification of the objective state.

To compare these two different systems quantitatively we ask the following question—for how much time T must the experiment be run to achieve a particular probability (say 99%) of identifying the objective state of the simulation with n number of sites?

Detection probability is taken as 99% for each atom. For the excitons we assume 90% detection probability here combining the effect of decay loss too. This is discussed and justified in detail in section 4.2.

A single experimental run time takes around 250 ms for the atoms [12] and estimated to be around 5 ns for the exciton. Assuming the above parameters, for the 50 site case, to get a 99% chance of the correct state occurring at least once, about 1.94 billion runs need to be made for the exciton case. This can be achieved in around 9.72 s. While for the atomic case only 842 runs are needed. However, due to the larger individual run times this would take around 210 s.

A smaller time for single experimental run lowers T by a fixed factor, while a better scaling of success probability with n (data in figure 4(a) of [12] for atoms and in figure 2(b) here for excitons) enhances T slower for higher n. Hence, the atomic system perform favorably for higher value of n (more number sites) while exciton system (in  $Cu_2O$ ) is faster for smaller n values.

It can be concluded from the above analysis that to scale to a really large number of sites, in the long term, one would actually need to improve line-separation vs linewidth ratio which differentiated the excitons from the atoms. This has been a problem in Cu<sub>2</sub>O system as other unwanted nearby states get excited which resulted in ineffective Rydberg excitation and correspondingly worse success probability scaling. In the Cu<sub>2</sub>O system, the small lifetime and the corresponding large linewidth of the Rydberg excitonic states caused this. Optical cavities could be used to enhance the coupling efficiency or to reduce the decay rate in such a system. This deserves a dedicated study to find optimal conditions for quantum nonlinear optics with Rydberg excitons. Another possible solution to this problem may be to use engineered micro structures to enhance the lifetime. Such a system has recently been experimentally demonstrated in the context of exciton condensation, in MoSe<sub>2</sub>–WSe<sub>2</sub> double layer material where the inter-layer excitons demonstrate long lifetimes and maintain the large binding energy which is required to observe and address Rydberg states [32]. Optical addressing and lifetime measurement of excitons in such structures have recently been studied in [33] with exciton lifetime of 0.2 ms. Although such long lifetimes may not actually be needed. Possibly a lifetime close to a microsecond would be enough as that would already mean a line separation vs linewidth ratio above 1000. However, there would be complications for long lifetimes as we would need trapping to keep the excitons in one place which would otherwise move due to thermal motion, discussed in details in section 4.4. However, there is an important difference with the trapped atoms. Rydberg excitons can be trapped mechanically using strain traps [24]. Such mechanical traps can be part of fabrication or prepared with the system. This would save precious trap preparation time for each iteration of the experiment, as needed for optical traps containing Rydberg atoms.

#### 4.2. Decay loss

There are two principal sources of loss in our system—decay loss and detection loss. Detection loss and ways to avoid it are presented in detail in section 4.3. The decay loss is caused by the decay of Rydberg states during the simulation. The objective state decays at a rate proportional to the number of excitons present. Thus given a fully connected ensemble in a regular polygon arrangement, the worst possible decay rate is proportional to 1/2 the size of the ensemble. For fewer Rydberg excitations, in partially connected ensembles, the effect of decay is even less. The low probability of Rydberg excitation at early part of the dynamics (see figure 2(a)) and our fast excitation timescales with respect to the lifetime allow us to reliably remove excitation decay from our numerical simulations for small number of sites. This helps to put computational resources toward treating higher number of qubits; see subsection 2.1 for our treatment of decay and position uncertainty. The objective state has a significant probability of being excited only

starting from 0.1 ns (see figure 2(a)). As the simulation ends at 0.24 ns, considering  $\sim$ 1 ns lifetime of the state, an individual exciton has a maximum of 14% chance of decay during simulation. However, this is only if an exciton is already excited by 0.1 ns, i.e. when the excitation probability is just picking up (as in figure 2(a)). On average, excitons would be excited much later and hence the decay probability would also be smaller. As a crude estimation, it can be considered around half of that ( $\sim$ 7%).

Given the size of the Hilbert space, solving the master equation for a 12-exciton site system is not possible with our numerical capabilities. To confirm our estimates we compared the results with and without decay for a four-exciton system in a polygon; see figure 3. As expected, the results support the reasoning above and show a manageable amount of reduction in the probability of success in reaching the target state.

Even then, for a large number of sites, exciton decay can no longer be neglected for theoretical simulation of the final state. However, for the practical purpose of detecting the objective state in an experiment, the exciton decay loss plays an equivalent role to the detection loss. The two losses manifest themselves differently—decay loss produces incorrect final states of simulation and detection loss inhibits the correct detection of the final state. But they both obstruct finding the objective state. With enough number of experimental runs one can find the objective state in the presence of each of the two losses. Hence, the maximum possible loss would simply be a combination of the two losses and the two losses can be treated equivalently for the purpose of finding the objective state; our prime goal in this proposal. Hence, even if we extrapolate our results for much larger number of sites (as we did for 50 sites using figure 2(b)) without considering the effect of exciton decay, we would still find the correct minimum probability of detecting the objective state(s) as long as we combine the decay loss with the corresponding detection loss.

#### 4.3. Detection

Faithful detection of the final state is an important requirement of our scheme. In the original detection scheme, we try to detect the  $|r\rangle = |25S\rangle$  state by making it decay and detecting emitted photon. However, |25s| state can only decay by two photon emission. Hence, as shown in figure 6(a) we transfer the |25s| state to  $|2P\rangle$  state by a THz detection laser and detect the photon emitted from the  $|2P\rangle$  state. This detection scheme completely depends on the ability to detect the one photon emitted from the  $|2P\rangle$  state. Even if one reaches a very high combined collection and detection efficiency (say, around 90%) of detecting the single photon or equivalently a single Rydberg excitation, the probability of detecting the final state decreases exponentially with larger number of excitons. Moreover, the large size of Rydberg excitons ( $\sim 1 \mu m$ ) compared to their blockade radius ( $\sim$ 2.82  $\mu$ m) means Rydberg excitation lasers (used for simulation) must be focused to a small area in the middle of the crystal resulting in excitation in a single exciton compared to a collective excitation over multiple excitons. Hence, there would be no preferred directions to the emitted photon in contrast to collective emission. This random direction of emission, coupled with limited coupling efficiency with the collecting fiber and finite detector efficiency lowers the photon detection efficiency. One way to enhance efficiency is using an optical cavity which would result in a directional emission even from a single exciton. Cavity would also enhance the coupling strength of the relevant exciton line while not enhancing the other off-resonant lines which would suppress the off-resonant excitations. However, fabricating such a cavity would also be challenging as it needs to have a quality factor in hundreds of thousands. It should be noted—as we have stressed before—low detection efficiency does not affect g<sub>2</sub> correlation function considerably as it is averaged over. High detection efficiency will become important for applications such as solving the MIS problem with tens or hundreds of nodes. It is also important to note that the high repetition rate in our proposal combined with detectors with low dark count will allows us to extend the experimental run time to converge on a solution.

To solve this problem, in the following we propose an alternate detection scheme which drastically improves the detection efficiency. Instead of directly detecting the Rydberg excitation by making it decay, here we detect the presence of the Rydberg state  $|r\rangle$  indirectly, as a non-demolition detection. The scheme is based on cyclic transitions as shown in figures 6(b) and (c). Detection lasers pulses are applied at all sites to create low lying Rydberg excitons (say,  $|12P\rangle$  state). We try to detect the emitted photons and the sequence is repeated.

In the absence of a Rydberg excitation (i.e. at the sites in  $|g\rangle$  state)  $|12P\rangle$  excitons would be created and decay by emitting photons (figure 6(c)). While in the presence of a Rydberg excitation (i.e. at the sites in  $|r\rangle$  state) excitation of  $|12P\rangle$  excitons will be inhibited due to the blockade effect (figure 6(b)). Such asymmetric Rydberg interaction (between two different Rydberg states) exists and has been observed between 6*P* and 17*P* states of Cu<sub>2</sub>O excitons. This was prominently seen in figure 3(e) of [16]. We expect a similar effect between  $|25S\rangle - |12P\rangle$  excitons will allow us to implement our proposed detection strategy. This would result in reduced excitation probability at a site in  $|r\rangle$  state compared to one in  $|g\rangle$  state. Hence  $|g\rangle$  and  $|r\rangle$  states can be easily distinguished if a large enough number of photons can be collected. The alternate detection

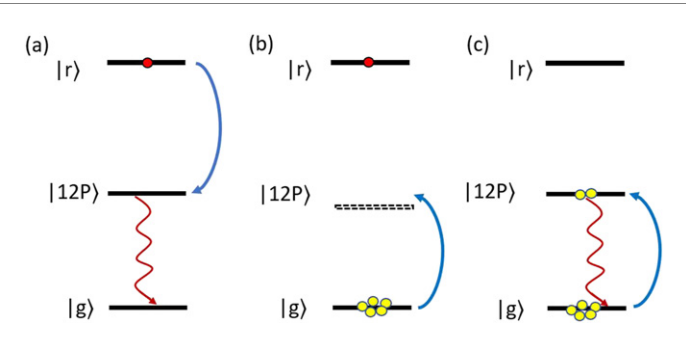


**Figure 6.** The two different detection schemes are shown. In the original scheme (a) Rydberg excitons in  $|r\rangle = |25S\rangle$  state are detected directly by first transferring it to (say),  $|12P\rangle$  state and then detecting the emitted photon. In the alternate scheme the presence of the  $|r\rangle$  state is detected indirectly, as a non-demolition detection, through many-body fluorescence detection. Detection laser pulse is applied to create shorter-lifetime and smaller-sized 12P excitons which decay by emitting photons that gets detected. The sequence is later repeated to detect a large number of photons from each site. Moreover, many P excitons are created at each site in each iteration as they are small in size compared to the  $|r\rangle$  exciton. Such P excitons are created if no  $|r\rangle$  exciton is present (b) but in presence of a  $|r\rangle$  exciton creation of P excitons gets hindered due to the blockade effect (c) resulting in lesser amount of photon emission. The detection protocol needs to have enough resolution to detect such reduced emission with high fidelity. See text for details.

scheme constitutes a non-demolition measurement of the Rydberg state. Although, it does constitute a measurement, e.g. destroying the coherence between two degenerate  $\mathbb{Z}_2$  eigenstates. P excitons are excited resonantly here, contrary to the two-photon excitation of S excitons, resulting in a phonon-assisted background absorption. However, the background is not significant compared to the transition line. It is complicated to include the exciton–phonon interaction in calculations. Hence, we neglect the effect of the background absorption in our calculation.

The relatively small energy gap between Rydberg states and the asymmetric Rydberg–Rydberg interaction raises a question whether all possible cross-interaction terms (n'S-nS for  $n' \neq n$ ) should also be included in equation (1). In this work, we minimized excitation in neighboring Rydberg states (where  $k \neq 25$ ) to eliminate the effect of such cross-interaction terms on the Rydberg population dynamics. For broadband addressing of Rydberg states and study of Rydberg exciton wavepacket dynamics, it is essential to include all potentially relevant cross-interaction terms. This novel complication introduces an opportunity to develop novel applications of Rydberg excitons in quantum information processing.

Note that the alternative detection scheme does not require a THz laser, only a yellow optical laser is needed. Also note that it is tricky to talk about  $|g\rangle$  state and  $|r\rangle$  state anymore as we are creating multiple excitons in the low lying p state. We discussed in introduction how multiple excitons can break our approximation of two level system. However, please observe that no additional  $|25S\rangle$  exciton is excited due to the blockade as before. So, for simplicity we will go on with the notation by redefining  $|g\rangle$  and  $|r\rangle$  state as absence and presence of  $|25S\rangle$  exciton only.

The principal advantage of the alternative detection scheme is that the number of photons collected from one site is huge as compared to maximum one in the original detection scheme. This is due to three reasons. Firstly, we perform a cyclic transition by repeatedly creating and detecting the  $|12P\rangle$  excitons. This can be repeated many times within the lifetime of the  $|25S\rangle$  exciton as the lifetime of  $|12P\rangle$  excitons are much smaller. Secondly, as the size of  $|12P\rangle$  excitons are much smaller than the  $|25S\rangle$  exciton many  $|12P\rangle$  excitons can be excited simultaneously which would result in detection of multiple photons each time. Thirdly, due to this ensemble excitation of  $|12P\rangle$  excitons the correspondingly emitted photons would be directional enhancing the photon collection efficiency. The above discussion implies that the lowest lying exciton states—which are smallest in size and have the shortest lifetimes—seemingly provide the most benefit for the detection scheme. However, the lowest lying states also have the least asymmetric Rydberg interaction with the 25S state, rendering the scheme invalid. Due to this trade-off the 12P state is considered. Please note that we assumed exciton linewidths to be radiative here, based on current evidences [16]. Although the contribution of phonon-mediated line broadening in excitons is not completely clear, especially to the lower n values. This may adversely affect the detection efficiency.

Asymmetric Rydberg interaction was explored in [16, 19]. The interaction coefficient between  $|n\rangle$  and  $|n'\rangle$  states is  $C_6 \propto n^7 n'^4$  if n < n' [19]. The corresponding blockade radius for continuous wave laser is given by  $r_{\rm bl} = (C_6/\gamma)^{1/6}$  where  $\gamma$  is the exciton radiative linewidth. Given  $\gamma \propto n^{-3}$ , blockade radius is given by  $r_{\rm bl} \propto (n^{10} n'^4)^{1/6}$ , where we have n=12 and n'=25. Comparing this blockade radius with the same state (n'-n'), with n'=25 blockade radius we have  $r_{\rm bl}^{(n,n')}/r_{\rm bl}^{(n',n')}=(n^{10}n'4/n'^{14})^{1/6}=(n/n')^{10/6}=(12/25)^{10/6}\approx 0.3$ . Although, this scaling formula is deduced using linewdith  $\gamma$ , the above formula holds for light pulses with Rabi frequency much larger than linewidth  $(\Omega)$  with  $\Omega\gg\gamma$ , say  $\Omega=10\gamma$ ) too, when such

a relation is used consistently to calculate both the blockade radius. For example, considering the earlier deduced blockade radius value—used in the simulation scheme— $r_{\rm bl}^{(25,25)}=2.82~\mu{\rm m}$ , the corresponding asymmetric blockade radius is  $r_{\rm bl(12,25)}=0.83~\mu{\rm m}$ . The corresponding Rabi frequency would be  $2\pi\times12.6~\rm GHz$ . A Rabi frequency larger than the linewidth is needed as the  $|12P\rangle$  excitons must be excited within a fraction of their decay time. However, a somewhat smaller Rabi frequency value—from the one used above—can be used to gain a bit more in blockade radius, which would be advantageous to the detection scheme. The above calculation is based on a rough estimate of asymmetric Rydberg interaction coefficient  $(C_6)$ . The asymmetric interaction coefficient,  $C_6$ , value  $(2\pi\times4.14~\rm GHz~\mu m^6)$  is found purely through n dependent scaling [19]—using the  $25S-25S~C_6$  value  $((2\pi\times706.09~\rm GHz~\mu m^6))$ —because only such an estimation was possible. Determining the exact asymmetric Rydberg interaction coefficients  $(C_6)$  is outside the scope of the current work.

We quantify the number of emitted photons from a site in  $|g\rangle$  state to show that indeed many photons are emitted. Lifetime of nth state is proportional to  $n^3$ . So, a transition to lower n levels can be repeated many times inside the lifetime of the  $|n=25\rangle$  state ( $\sim$ 9 times to n=12 state). Moreover, the size of lower lying excitons are much smaller, given by spherical volumes with radius  $\langle r_n \rangle = \frac{1}{2} a_{\rm B} (3n^2 - l(l+1))$ , where Bohr radius  $a_B = 1.11$  nm and for s excitons l = 0 while for p exciton states l = 1. This gives a radius of 238.7 nm for 12P states. Considering the asymmetric blockade radius of 830 nm (estimated above) and assuming we wait for two lifetimes (of P state) to let all the excitons emit, a total number of  $(830/238)^3 \times 9/2 = 192$  photons can be emitted from the blockade volume through our detection scheme, when no Rydberg exciton is excited (i.e., for figure 6(b)). The goal of the detection scheme is to distinguish between the presence and absence of a Rydberg exciton (in  $|r\rangle = |25S\rangle$  state). In presence of the Rydberg exciton generation of excitons within the blockade volume gets inhibited. We estimated the corresponding number of photon emission that will be inhibited above. However, the total number of emitted photons would be greater as the detection beam would generate excitons outside the blockade volume too as it passes through the crystal. If we consider a cylindrical volume with radius  $\sim 1~\mu m$  and length 4  $\mu m$  (crystal thickness) then the total enclosed volume would be about five times the blockade volume. Hence, the total number of photons emitted, in absence of an exciton in  $|r\rangle$  state, is five times more or  $\sim$ 1000 photons. In presence of an exciton in the  $|r\rangle$  state, the number of emitted photons would be reduced to around 800–900 photons depending on how many excitons within the blockade volume (estimated previously to be  $\sim$ 190) or in nearby areas are successfully blockaded by the Rydberg interaction. In reality, the total number of emitted photons (estimated  $\sim$ 1000) can be reduced further too while keeping the photon number emitted within the blockade volume by simply focusing the beam in the middle of the crystal. Then the exciton generation probability closer to the surface of the crystal reduces but the probability remains high at the middle around the blockade volume. This would be advantageous for the detection protocol as the contrast in photon numbers between presence and absence of an Rydberg exciton (in |25S) state) will grow further.

We estimated the mean emitted photon number above. But to distinguish between the  $|g\rangle$  and  $|r\rangle$  states by measuring photon number, we need to know the photon number distribution too. We assume the probability to successfully detect a particular exciton by photon detection is P—i.e. combining probabilities of photon emission within the detection time window, within the spatial collection angle and successful detection. If a total N number of excitons are attempted to be detected (in time and space), their distribution is binomial resulting in mean photon detected  $\overline{x}=Np$  and variance  $\sigma^2=Np(1-p)$ . As binomial distributions are almost Gaussian for high N, a  $4\sigma$  mean separation between the two distribution (corresponding to the  $|g\rangle$  and  $|r\rangle$ ) will mean a very small overlap (less than 3%) between them. As  $\sigma\ll\overline{x}$  in our case we can assume both  $\sigma$  and  $\overline{x}$  to be almost same for both distribution. A  $4\sigma$  separation would imply, detection fidelity of 97.5%. Assuming a photon collection probability of p=0.5 for N=1000, the mean number of detected photon  $\overline{x}=500$  with  $\sigma\sim16$ . This implies that according to the above rough estimate the detection scheme can achieve above 97% fidelity if the asymmetric blockade effect reduces detected photons by 64 and correspondingly emitted photons 128 (considering p=0.5 detection probability). We estimated that the blockade volume will contain around 190 photons. Hence, it is conceivable that the above detection fidelity can be achievable.

We did not consider the effect of the decay of the Rydberg state on our alternative detection scheme yet. When the Rydberg state decays, the blockade effect goes away and there is no more suppression of photon emission. Hence, it seems best to detect early so that no Rydberg state decays. However, if we do not wait for long enough then there is not enough photons and we cannot distinguish as seen above. Hence, there is an optimal time to stop detection which we found out to be  $0.5 \times$  decay time. Decreasing the detection time by half adversely affects the above estimate but not by a lot, especially given the small difference of photon number required in our scheme.

### 4.4. Other implementation details

We now discuss several details of our proposal. We chose nS Rydberg states because it offered two important simplifications in tracking the quantum dynamics. nS states have only one angular momentum state  $|n00\rangle$  and hence the product state  $|n00\rangle|n00\rangle$  is the eigenstate of the non-interacting Hamiltonian [18]. Also, owing to the zero angular momentum nS states does not have any angle dependence in Rydberg interaction coefficients. Hence, for a polygon configuration of sites (figure 1(c)) or even an arbitrary configuration (as explored in figure 5 for MIS problem) the Rydberg interaction and the corresponding evolution is tractable for nS states (for up to 12 sites using computer systems available to us).

Although *nP* states can be excited directly by one yellow laser and offer an experimentally simpler scenario, *nP* states introduce considerable complications in tracking the quantum simulation. This includes angle-dependent Rydberg–Rydberg interaction and difficulty in exciting eigenstates of the Rydberg interaction Hamiltonian, which in this case are mostly entangled states [18].

For these reasons, we choose to address *nS* states and take advantage of the additional flexibility in the geometry to apply this system to applications such as solving the MIS problem. However, the superposition states holds promise for potential non-trivial many-body quantum dynamics to be explored. In this context, many-body quantum dynamics of Rydberg exciton has recently been explored in [27].

In the proposed experiment, we intend to excite the n=25 excitation with about 1  $\mu$ m radius and about 3  $\mu$ m blockade radius. Hence to prevent double excitons occurring along the crystal propagation direction the crystal needs to be rather thin, around 3–4  $\mu$ m. It is a challenge to manufacture such small thickness artificial Cu<sub>2</sub>O crystals, although artificial Cu<sub>2</sub>O micro-crystals has recently been created [23]. Another problem with using a small thickness crystal is that it can change the energy level structure of the excitons, because it is now confined inside a potential well. Considering these issues, a little more thickness would actually probably be fine as the laser itself is focused in about 1–2  $\mu$ m length at the center of the crystal and hence weaker in intensity at the edges, resulting in larger blockade radius there.

We have calculated such energy changes considering the finite confinement potential well as perturbation. The potential barrier of the confinement well has an energy of 2.98 eV, which can be found by subtracting the Rydberg energy (of 2.17 eV) from the Cu<sub>2</sub>O work function energy (of about 5.15 eV) [34]. Given the energy separation between n=24 and n=25 states is around 15  $\mu$ eV, energy changes are prominent if the thickness is below 3.5  $\mu$ m (about 12  $\mu$ eV energy shift to n=25 level for 3.5  $\mu$ m thickness) while negligible above 4  $\mu$ m (about 9 × 10<sup>-4</sup>  $\mu$ eV for 4  $\mu$ m thickness).

There is also a possibility that the excitons could move due to thermal motion despite the very small timescales used. This would be detrimental to our proposal. However, we estimated that in the simulation duration of  $\sim$ 0.2 ns and at 1 K temperature, even if an exciton moves ideally, uninhibited with its average thermal velocity, it would only travel  $\sim$ 1  $\mu$ m. Moreover, in practical systems there is scattering due to crystal imperfection which would further slow down the exciton greatly. Also, the system can be cooled to mK temperatures to constrain the exciton motion even more.

# 5. Conclusions

In conclusion, we simulated many-body Rydberg excitation dynamics in  $Cu_2O$  excitons. Despite the detrimental effect of neighboring Rydberg states, we demonstrated that  $\mathbb{Z}_2$ -ordered phase can be reached and observed using correlation in detected emission. We explored the scaling of the success probability and showed that such many-body quantum states can be reached and observed for over 50 exciton sites at experimental run times two orders of magnitude shorter than the individually trapped Rydberg atoms. Using the ability to selectively excite excitons in an arbitrary configuration, we argued MIS problems can be solved in the Rydberg exciton system. To further scale up the system, we discussed the possibility of improving exciton lifetimes by many orders of magnitude using engineered 2D micro structures. Overall these results show the potential of  $Cu_2O$  excitons and other attractive semiconductor systems for Rydberg excitons to be used to simulate many-body dynamics with applications extending to complex optimization problems.

# Acknowledgments

SG acknowledges support through an Alberta Innovates Technology Futures (AITF) Graduate Student Scholarship (GSS), an Izaak Walton Killam Doctoral Scholarship and an Eyes High International Doctoral Scholarship of University of Calgary. CS and KH acknowledge support from the Natural Sciences and Engineering Research Council (NSERC) of Canada through Discovery Grants. CS also acknowledges support from NSERC's support through the CREATE program.

## Data availability statement

All data that support the findings of this study are included within the article (and any supplementary files).

#### **ORCID** iDs

Khabat Heshami https://orcid.org/0000-0003-3864-1930

#### References

- [1] Saffman M, Walker T G and Mølmer K 2010 Rev. Mod. Phys. 82 2313
- [2] Šibalić N and Adams C S 2018 Rydberg Physics (Bristol: IOP Publishing) pp 2399-891
- [3] Urban E, Johnson T A, Henage T, Isenhower L, Yavuz D D, Walker T G and Saffman M 2009 Nat. Phys. 5 110
- [4] Gaëtan A, Miroshnychenko Y, Wilk T, Chotia A, Viteau M, Comparat D, Pillet P, Browaeys A and Grangier P 2009 Nat. Phys. 5 115
- [5] Peyronel T, Firstenberg O, Liang Q-Y, Hofferberth S, Gorshkov A V, Pohl T, Lukin M D and Vuletić V 2012 Nature 488 57
- [6] Müller M, Kölle A, Löw R, Pfau T, Calarco T and Montangero S 2013 Phys. Rev. A 87 053412
- [7] Paredes-Barato D and Adams C 2014 Phys. Rev. Lett. 112 040501
- [8] Gorniaczyk H, Tresp C, Schmidt J, Fedder H and Hofferberth S 2014 Phys. Rev. Lett. 113 053601
- [9] Kómár P, Topcu T, Kessler E, Derevianko A, Vuletić V, Ye J and Lukin M 2016 Phys. Rev. Lett. 117 060506
- [10] Han Y, He B, Heshami K, Li C-Z and Simon C 2010 Phys. Rev. A 81 052311
- [11] Zhao B, Müller M, Hammerer K and Zoller P 2010 Phys. Rev. A 81 052329
- [12] Bernien H et al 2017 Nature 551 579
- [13] Keesling A et al 2019 Nature 568 207
- [14] Omran A et al 2019 Science **365** 570
- [15] Pichler H, Wang S-T, Zhou L, Choi S and Lukin M D 2018 arXiv:1808.10816
- [16] Kazimierczuk T, Fröhlich D, Scheel S, Stolz H and Bayer M 2014 Nature 514 343
- [17] Heckötter J, Freitag M, Fröhlich D, Aßmann M, Bayer M, Semina M A and Glazov M M 2017 Phys. Rev. B 96 125142
- [18] Walther V, Krüger S O, Scheel S and Pohl T 2018 Phys. Rev. B 98 165201
- [19] Heckötter J, Walther V, Scheel S, Bayer M, Pohl T and Aßmann M 2021 Nat. Commun. 12 3556
- [20] Mund J, Fröhlich D, Yakovlev D R and Bayer M 2018 Phys. Rev. B 98 085203
- [21] Farenbruch A, Mund J, Fröhlich D, Yakovlev D R, Bayer M, Semina M A and Glazov M M 2020 Phys. Rev. B 101 115201
- [22] Kang D D, Gross A, Yang H, Morita Y, Choi K S, Yoshioka K and Kim N Y 2021 Phys. Rev. B 103 205203
- [23] Steinhauer S, Versteegh M A, Gyger S, Elshaari A W, Kunert B, Mysyrowicz A and Zwiller V 2020 Commun. Mater. 1 11
- [24] Krüger S O and Scheel S 2018 Phys. Rev. B 97 205208
- [25] Khazali M, Heshami K and Simon C 2017 J. Phys. B: At. Mol. Opt. Phys. 50 215301
- [26] Walther V, Johne R and Pohl T 2018 Nat. Commun. 9 1309
- [27] Poddubny A N and Glazov M M 2019 Phys. Rev. Lett. 123 126801
- [28] Uihlein C, Fröhlich D and Kenklies R 1981 Phys. Rev. B 23 2731
- [29] Walther V, Grünwald P and Pohl T 2020 Phys. Rev. Lett. 125 173601
- [30] Schöne F, Stolz H and Naka N 2017 Phys. Rev. B 96 115207
- [31] Pichler H, Wang S-T, Zhou L, Choi S and Lukin M D 2018 arXiv:1809.04954
- [32] Wang Z, Rhodes D A, Watanabe K, Taniguchi T, Hone J C, Shan J and Mak K F 2019 Nature 574 76
- [33] Montblanch A et al 2021 Commun. Phys. 4 119
- [34] Konzelmann A, Frank B and Giessen H 2019 J. Phys. B: At. Mol. Opt. Phys. 53 024001